Title

Laminin N-terminus α31 expression during development in an inducible-transgenic mouse model is lethal and causes a multitude of tissue-specific defects

Author names and affiliations

Conor J. Sugden, Valentina Iorio, Lee D. Troughton, Ke Liu, George Bou-Gharios*, Kevin J. Hamill*

*these authors jointly supervised this work

Corresponding author (name and permanent address)

Kevin J Hamill

William Henry Duncan Building,

University of Liverpool,

6 West Derby Street,

Liverpool, UK

L7 8TX

Abstract

Alternative splicing of the laminin α3 gene gives rise to a netrin-like protein termed LaNt α31, the major structural feature of which is a laminin N-terminal domain. LaNt α31 is expressed across a wide range of tissues, is upregulated in cancers, and ex vivo and in vitro functional studies have indicated that this relatively unstudied protein influences wound repair, stem cell activity, and tumour progression via modifying matrix organisation. However, LaNt α31 functionality has never been investigated in vivo. Here we report the generation and characterisation of the first LaNt α31 transgenic mouse line using the ubiquitin C promoter to drive expression of an expression cassette containing a flox-STOP sequence, the human LaNt α31 coding sequence and a tdTomato reporter. This line was crossed with mice expressing inducible Cre recombinase driven from the Rosa26 locus (R26CreERT2), and double transgenics were given tamoxifen at E15.5 to induce expression. LaNt α31 overexpressing animals were fully formed and intact at birth but were not viable, exhibiting localised regions of erythema. Histological examination revealed numerous striking defects includng extra-vascular erythrocytes across multiple tissues. Widespread disorganisation was apparent in the kidney, with epithelial detachment, tubular dilation, interstitial bleeding observed, and thickening of the kidney tubule basement membranes. In the skin, mice exhibited disruption of the epidermal basal cell layer and hair follicle outer root sheath, with evidence of basement membrane interruption in the interfollicular epidermis. In the liver, there was a ~50% reduction of total cell number, associated with a depletion of hematopoietic erythrocytic foci. In the lungs, there appeared to be a reduction of alveolar epithelial cells accompanied by blood interspersed throughout the tissue. Together, these findings demonstrate that LaNt α31 can influence tissue morphogenesis during development and implicate this new protein as a potentially important mediator of basement membrane assembly.

Keywords (max 6)

Laminin, netrin, basement membrane, development

Abbreviations

LaNt α31, laminin N-terminus α31; BM, basement membrane; ECM, extracellular matrix; LN, laminin N-terminal; LM, laminin; LE, laminin-type epidermal growth factor-like domain; DMEM, Dulbecco's Modified Eagle Medium; SDS-PAGE sodium dodecyl sulfate polyacrylamide gel electrophoresis; mEFs, mouse embryonic fibroblasts; hK14, human keratin 14; intraperitoneal injection, IP

Introduction

Basement membranes (BMs) are specialised extracellular matrix (ECM) structures with essential and remarkably diverse roles in most cell and tissue behaviours; including regulating differentiation, cell adhesion and migration [1, 2]. BMs not only provide the mechanical attachment points that support sheets of cells to resist stresses but also influence signalling cascades via direct binding to cell surface receptors, through the sequestration and controlled release of growth factors, and by providing biomechanical cues, as reviewed in [3, 4]. BMs are also dynamic structures that are remodelled in terms of composition and structure throughout life, with the most striking changes occuring during development [5, 6]. At the core of every BM are two networks of structural proteins; type IV collagens and laminins (LMs)[7].

Each LM is an obligate αβγ heterotrimer formed from one of five α chains (LAMA1-5), three β chains (LAMB1-3) and three γ chains (LAMC1-3), with each chain displaying spatio-temporal distribution patterns, as reviewed in [8-11]. Assembly of LM networks and higher-order structures involves formation of a ternary node between the laminin N-terminal (LN) domains of an α, a β and a γ chain [12, 13]. These ternary αβγ nodes assemble in a two-step process involving an initial rapid formation of unstable βγ LN intermediate which is then stabilised through the incorporation of an α LN domain [14-17]. The biological importance of these LN-LN interactions is exemplified by a group of human syndromic disorders where missense mutations affecting the LN domains of the LAMA2, LAMB2 or LAMA5 genes give rise to muscular dystrophy in merosin-deficient muscular dystrophy, kidney and ocular developmental defects in Pierson syndrome, or defects in kidney, craniofacial and limb development respectively [18-22]. Although these disorders demonstrate that LM network assembly is essential for homeostasis of numerous tissues, not all LM chains contain an LN domain. Specifically, LMα4, which is expressed at high levels in the vasculature, and the

LMα3a and LMγ2 chains, which are abundant in surface epithelium including the skin, have shortened amino termini which lack this key domain but yet still form functional BMs [8, 9, 23, 24]. This raises questions of whether LN domains are important in all tissue contexts or whether additional proteins may compensate for the inability of the LMs to form networks.

Alongside their main LM transcripts, the LAMA3 and LAMA5 genes produce short transcripts encoding proteins that are unable to trimerise into LMs but which contain LN domains [25]. At least one of these laminin N terminus proteins encodes a functional protein, LaNt α31, the structural features of which are an α LN domain followed by a short stretch of laminin-type epidermal growth factor-like (LE) domains and unique C-terminal region with no conserved domain architecture. In addition to the LaNt proteins, the laminin-superfamily includes netrin genes which encode proteins with either β or γ LN domains, stretches of LE repeats and unique C-terminal regions (as reviewed in [26]. Moreover, proteolytic processing of LMs are also released from LMα1 [27], LMβ1 [28], LMα3b [29]. Each of these LN domain-containing proteins and cryptic fragments have cell surface receptor binding capabilities and can act as signalling molecules (reviewed in [30]. However, netrin-4, which evolved independently from the other netrins [31, 32], also has LM-network disrupting capabilities [33, 34], and when overexpressed in vivo, caused increased lymphatic permeability [35]. Netrin-4 LN domain has greatest homology with LM β LN domains whereas LaNt α31 contains the LMα3b LN domain [36]; therefore, although LaNt α31 could act similarly to these proteins, it likely plays a different role depending on the LM context.

LaNt α31 is expressed in the basal layer of epithelia in the skin [25], cornea [37] and digestive tract, the ECM around terminal duct lobular units of the breast and alveolar air sacs in the lung, and is widely expressed by endothelial cells [38]. Increased expression is associated with breast ductal carcinoma and in vitro overexpression leads to a change in the mode of breast cancer cell invasion through LM-rich matrices [39]. LaNt α31 is also

transiently upregulated during re-epithelialization ex vivo burn wounds and in stem cell activation assays [37]. In epidermal and corneal keratinocytes, knockdown or overexpression experiments revealed that modulating LaNt α31 levels leads to reduced migration rates and modifying cell-to-matrix adhesion [25, 40]. Consistent with a role in matrix assembly, increased expression LaNt α31 causes striking changes to LM332, including formation tight clusters beneath cells and increasing the proteolytic processing of LMα3 by matrix metalloproteinases [40]. Although these findings all support LaNt α31 as being a mediator of cell behaviour, it is as yet unknown what role it plays in complex in vivo tissue environments and in particualar in matrixes that are actively being remodeled.

Here, we present the first in vivo study of LaNt α31 overexpression in newly developed mouse models.

Results

Inducible LaNt α31 construct validation.

To investigate the consequences of LaNt α31 overexpression in vivo, we generated an inducible system for conditional LaNt α31 transgene expression (figure 1A). An expression construct was created containing the ubiquitin C promoter driving expression of the human LaNt α31 cDNA with the native secretion signal replaced by mouse immunoglobulin κ leader sequence to maximise scretion, and with sequences for Flag and HA epitope tags added to the C-terminus of the LaNt α31 coding region. A T2A element was included to enable expression of tdTomato from the same transgene but not directly fused to LaNt α31 [46]. A floxed stop-cassette was inserted between the promoter and the start of the construct to prevent transgene expression until Cre-mediated removal of this cassette. The entire construct was flanked with the cHS4 β-globin insulator to protect against chromatin-mediated gene silencing [52] (figure 1A). Restriction enzyme digests and plasmid sequencing confirmed the assembled pUbC-LoxP-LaNtα31-T2A-tdTomato plasmid.

To confirm the construct expressed only following exposure to Cre recombinase, the pUbC-LoxP-LaNtα31-T2A-tdTomato was co-transfected alongside pCAG-Cre:GFP, encoding GFP-tagged Cre recombinase, into HEK293A cells. tdTomato signal was observed only in cells transfected with both plasmids (figure 1B). PCR using primers flanking the STOP cassette also confirmed that the cassette was removed only in cells transfected with both plasmids (figure 1C). Western blotting using polyclonal anti-Flag antibodies confirmed expression of the predicted ~ 57 kDa band in co-transfected cell lysates (figure 1D), this also confirmed that the T2A element was cleaved in the final product releasing the tdTomato tag. Together, these results demonstrate that the pUbC-LoxP-LaNtα31-T2A-tdTomato plasmid allows for the Cre-inducible expression of LaNt α31 and tdTomato.

Generation and validation of a novel LaNt α31 overexpressing mouse line.

The pUbC-LoxP-LaNtα31-T2A-tdTomato construct was linearised, and transgenic F0 mice generated by pronuclear microinjection into oocytes. To confirm transgene expression, F0 mice were mated with WT (C57BL/6J) mice, embryos were collected at E11.5, and mEFs were isolated from the embryos. Presence of the UbC-LoxP-LaNtα31-T2A-tdTomato transgene (hereafter UbCLaNt) was confirmed by PCR (figure 2A). mEFs were transduced with an adenovirus encoding codon-optimised Cre recombinase (ad-CMV-iCre). Analysis by immunoblotting with anti-HA-antibodies (figure 2B) revealed a ~57 KDa band and fluorescence microscopy confirmed tdTomato expression (figure 2C) in samples containing both the UbC-LaNt transgene and the ad-CMV-iCre, but not in cells with either plasmid individually.

Male UbCLaNt mice were mated with females from the tamoxifen-inducible ubiquitous Cre line R26CreERT2 (figure 3A). Transgene expression was induced by IP of tamoxifen at E13.5, and embryos collected at E19.5. PCR confirmed that Cre/LoxP mediated recombination only occurred in the embryos with both the UbCLaNt and the R26CreERT2 (figure 3B). Explants were generated from the skin of these embryos, and only the explants grown from double transgenic embryos exhibited tdTomato expression by fluorescence microscopy (figure 3C) and HA-tagged LaNt α31 expression by western immunoblotting (figure 3D). Together, these data confirmed the generation of tamoxifen-inducible LaNt α31 overexpressing mouse line, without detectable leakiness (UbCLaNt::R26CreERT2).

UbCLaNt::R26CreERT2 expression in utero causes death and localised regions of erythema at birth.

To determine the impact of LaNt α31 during development where extensive BM remodelling occurs, tamoxifen was administered via IP to pregnant UbCLaNt::R26CreERT2

mice at E15.5 and pregnancies allowed to continue to term. Across two litters from different mothers, two from six pups and three from five pups respectively were intact but not viable at birth, while the remaining littermates were healthy. The non-viable pups displayed localised regions of erythema with varying severity between the mice, but were otherwise fully developed and the same size as littermates (figure 4A). Genotyping identified that all offspring possessed both the UbCLaNt and R26CreERT2 transgenes (figure 4B). Hereafter, non-viable pups are referred to as UbCLaNt::R26CreERT2 1E1, 1E2, 2E1, 2E2, 2E3, and viable pups UbCLaNt::R26CreERT2 2NE1, 2NE2. To confirm transgene expression, skin explants were established from non-viable pups, and tdTomato fluorescence was confirmed by microscopy (figure 4C). Consistent with the fluorescence data, western immunoblot analysis of total protein extracts from the explanted cells and whole embryo lysates revealed transgene expression in non-viable pups, although expression levels varied between the mice (figure 4D). To further confirm transgene expression within tissues, OCT-embedded skin sections of UbCLaNt::R26CreERT2 were processed with anti-mCherry antibodies which recognise the tdTomato protein, revealing that only the non-viable pups expressed the tdTomato reporter (figure 4E). Together these data confirm that only non-viable mice expressed the LaNt α31 transgene

To identify LaNt α31 effects at the tissue level, the pups were formalin-fixed and paraffin-embedded then processed for H&E and immunohistochemistry. All organs were present in the mice and appeared intact at the macroscopic level; however, blood exudate was observed throughout multiple tissues in all of the LaNt α31 transgene expressing mice. We focused our attention on kidney, skin and lung as examples of tissues where the BMs with differences in LM composition and where we hypothesised LaNt α31 could, therefore, elicit distinct effects. Specifically, the predominant LMs in the kidney contain three LN domains, and mutations affecting LM polymerisation lead to Pierson syndrome [19, 53-56], whereas

the major LM in the skin contains one LN domain, LM332, and loss of function leads to skin fragility, reviewed in [57], and granulation tissue disorders [58, 59]. In the lung, LM311, a two LN domain LM, is enriched [60, 61] and absence of LMα3 is associated with pulmonary fibrosis [62]. Each of these three tissues also express LaNt α31 in adult human tissue, and are, therefore, tissues where dysregulation of expression regulation could be physiologically relevant [38].

LaNt α31 overexpression leads to epithelial detachment, tubular dilation and interstitial bleeding in the kidney.

In the kidneys, striking alterations were observed in the renal tubules, pelvis, and blood vessels of UbCLaNt::R26CreERT2 mice expressing the transgene. Specifically, dilation and detachment of the lining epithelia in collecting ducts and uteric bud segments was evident (figure 5, black arrows), and changes were observed in the vessels of the kidney, with bleeding into the interstitial and subtubular surroundings (figure 5, yellow arrows). There was some severity in the extent of the defects between the expressing pups (interstitial bleeding 4 out of 5 mice, pelvic dilation 2 out of 5, epithelial detatchment and tubular observed in all mice). Indirect IF processing of tissue using antibodies raised against LM111 revealed LM localisation to be unchanged, however immunoreactivity of the tubule BMs was thickened in the expressing pups compared with littermate controls (figure 6).

LaNt α31 overexpression disrupts epithelial basal cell layer organisation.

Histological examination of the dorsal skin of UbCLaNt::R26CreERT2 mice revealed localised disruption of the epidermal basal cell layer, with a loss of the tight cuboidal structure of the stratum basale (figure 7A). Basal layer disruption was also observed in the outer root sheath of the hair follicles (figure 7A). Although no evidence of blistering at the

dermal-epidermal junction was observed Mice expressing the LaNt α31 transgene displayed discontinuous LM immunoreactivity at the epidermal-dermal junction (figure 7B). However, the LM surrounding the outer root sheath was unaffected (figure 7B)..

Mice expressing the LaNt α31 transgene display structural differences in the lung.

Lungs of P0 mice were not inflated prior to FFPE, however structural differences between non-expressing and expressing mice were apparent. Specifically, in mice expressing LaNt α31, fewer, less densely packed alveolar epithelial cells were observed. Additionally, and similarly to the kidney, erythrocytes were present throughout the lung tissue. (figure 8).

LaNt α31 overexpression leads to a reduction of hematopoietic colonies in the liver.

Surprisingly, drastic and obvious superficial changes were apparent in the livers of mice expressing the LaNt α31 transgene compared to the non-expressing mice. Although the bile ducts, sinusoid endothelium and hepatocyte morphology were unchanged, there was a clear reduction in hematopoietic foci in the LaNt α31 transgene expressing animals (figure 9A). This reduction corresponded to a >48% reduction of total cell number (WT= 11.5 nuclei/mm^2, mean NE = 11.4 nuclei/ mm^2, mean E= 5.8 nuclei/mm^2; figure 9B).

Keratin 14-driven constitutive LaNt α31 induces a low offspring number.

We next used a keratin-14 promoter (K14) to restrict expression to skin and the epithelia of tongue, mouth, forestomach, trachea, thymus and respiratory and urinary tracts [63-65]. K14 promoter activity has also been described in the oocyte [66]. The new construct used the human K14 promoter drive expression of human LaNt α31, followed by a T2A element and a mCherry reporter (supplemental figure 1A) and was validated by transfecting into KERA 308 mouse epidermal keratinocytes and visualising the mCherry fluorescence

(supplemental figure 1B) and immunoblotting for the LaNt α31 protein (supplemental figure 1C).

K14-LaNtα31 transgenic mice were generated by pronuclear microinjection. However, unusually small litters were obtained from recipient CD1 mothers and mice containing the transgene DNA (supplemental figure 1D) did not express the transgene at the protein level (supplemental figure 1F-G). The unusually low offspring sizes, combined with the lack of protein expression in genotype-positive mice, suggests that expression of LaNt α31 under the control of the K14 promoter is lethal during development.

Discussion

This study has demonstrated that LaNt α31 overexpression ubiquitously during development is embryonically lethal and causes an array of tissue specific-defects. These include blood exudate throughout most tissues as well as striking changes to the tubules of the kidney and the basal layer of the epidermis, depletion of hematopoietic colonies in the liver, and evidence of BM disruption was apparent at the dermal-epidermal junction. These findings build upon in vitro and ex vivo work that have implicated LaNt α31 in modulating cell adhesion, migration, and LM deposition [25, 37, 40], and for the first time demonstrates that this little-known LAMA3-derived splice isoform plays a role in BM and tissue homeostasis during development.

As LM network assembly requires binding of an α, β and γ LN domain [14-17, 67], we predicted that the presence of an α LN domain within LaNt α31 would influence LM-LM interactions and therefore BM assembly or integrity. Consistent with this hypothesis, much of the UbCLaNt::R26CreERT2 mice phenotypes resemble those from mice where LM networks cannot form due either to LN domain mutations or overexpression of the LM-network disrupting protein, netrin-4. Specifically, mice with a mutation in the LN domain of LM α5 die before birth exhibiting defective lung development and vascular abnormalities in the kidneys [68]. While mice with LM β2 LN domain mutations or LN domain deletions exhibit renal defects, and although viable at birth, become progressively weaker and die between postnatal day 15 and 30 [69-74]. Additionally, mice with netrin-4 overexpression under the control of the K14 promoter were born smaller, redder, and with increased lymphatic permeability [35]. In comparison to each of these lines, the LaNt α31 animals present with similar but more severe and more widespread phenotypes, which reflects the more widespread UBC and R26 promoter activities. Nevertheless, based on the broad similarity between these phenotypes, we propose a model where LaNt α31 overexpression inhibits LM

network assembly by competing with the native LM α chain. However, within this model, there remains the question of how LaNt α31 influences tissues where there the expressed LMs do not contain an α LN domain, and therefore are not able to polymerise [16]. For example, The LM composition present within vessel BMs during development and lymph vessels is rich in the β and γ LN domain-containing LM411 [75-77]. Here, one might have anticipated that the LaNt α31 LN domain could stabilise weak βγ LN dimers strengthening the BM but the observed phenotype of blood exudate throughout the mouse tissues suggests instead that the LaNt α31 transgenics have vascular leakage which overall points to a disruptive rather than stabilising role.

Although the in vivo findings presented here along with previous in vitro studies both strongly support LaNt α31 acting as a regulator of BM homeostasis we cannot fully rule out the possibility of LaNt α31 acting as a signalling protein [25, 37, 39, 40]. Specifically, integrin-mediated signalling from LaNt α31-like proteolytically released LN-domain containing fragments from LM α3b, α1, and β1 chains have been reported [27-29] and some aspects of the UbCLaNt::R26CreERT2 phenotype are consistent with LaNt α31 acting in this way. For example one of the most striking phenotypes observed in the UbCLaNt::R26CreERT2 mice was the depletion of hematopoietic colonies in the liver, an essential stem cell niche during development [78-80]. Integrins α6 and β1 are highly expressed in hematopoietic stem cells, and are central to the process of migration both in and out of the fetal liver [81-83], and a netrin-4/laminin γ1 complex has been shown to signal through the integrin α6β1 receptor [84]. Indeed,LaNt α31 may signal in a similar manner, which may be detrimental to the maintenance of hematopoietic colonies in the fetal liver. However, altering LM network structural organisation also changes outside-in signalling, through direct changes to the presentation of ligands, and through modifying BM growth factor sequestration or release [85]. LMs networks are also critical for maintaining progenitor

303 cell “stemness” [86-89]. Intriguingly, we previously identified that LaNt α31 is enriched in
304 limbal stem cell niche of adult corneas and that expression was further upregulated upon ex
305 vivo stem cell activation or during wound repair [37]. Coupled to the striking phenotype
306 observed here, it is tempting to hypothesise that LaNt α31 is either directly or indirectly
307 involved in regulating stem cell quiescence.

308 In the present study, expression was induced during development to focus expression
309 to times when basement membrane remodelling is highly active and thereby maximising the
310 opportunity to observe a phenotype. Considering the widespread expression of LaNt α31
311 [38], and the dramatic effects observed in this study, it will be interesting to determine effects
312 in adult animals. For example, LM network integrity is critical to muscle function, with LM
313 α2 LN domain mutations or deletions developing muscular dystrophy and peripheral
314 neuropathy over time [90-92], therefore although no overt muscle phenotype was observed in
315 the new-born LaNt α31 transgenic animals, longer-term studies may reveal further
316 phenotypes once tissues are placed under stress. As the LaNt α31 phenotypes are deleterious,
317 further studies will require lineage-specific expression to gain deeper cellular and temporal
318 resolution.

319 This study provides the first in vivo evidence that LaNt α31, the newest member of
320 the LM superfamily, is a biologically relevant matricellular protein and further emphasises
321 the importance of LN domains as regulators of tissue homeostasis. Importantly, while
322 disease-causing LN domain mutations are rare in normal biology, changes to alternative
323 splicing events often occur in normal situations, including development and wound repair,
324 and in pathological situations including cancer [93-95]. Taken together, these findings have
325 exciting amd potentially far reaching implications for our understanding of BM biology.
326

Methods

Ethics

All procedures were licensed by the UK Home Office under the Animal (Specific Procedures) Act 1986, project license numbers (PPL) 70/9047 and 70/7288. All mice were housed and maintained within the University of Liverpool Biological Services Unit in specific pathogen-free conditions in accordance with UK Home Office guidelines. Food and water were available ad libitum.

Antibodies

Rabbit monoclonal antibodies against the influenza hemagglutinin epitope (HA) (C29F4, Cell Signalling Technology, Danvers, MA) were used for immunoblotting at 67 ng/ml. Goat polyclonal antibodies against DDDDK (equivalent to FLAG sequence, ab1257, Abcam, Cambridge, UK), rabbit polyclonal antibodies against 6X-His (ab137839, Abcam), and rabbit polyclonal antibodies against lamin A/C (4C11, Cell Signalling Technology) were used at 1 µg/ml for immunoblotting. Mouse monoclonal antibodies against LaNt α31 [37] were used at 0.225 µg/ml for immunoblotting. Rabbit polyclonal antibodies against mCherry (ab183628, Abcam) were used at 2.5 µg/ml for immunofluorescence. Aexa fluor 647 conjugated goat anti-rabbit IgG recombinant secondary antibodies, were obtained from Thermo Fisher Scientific (Waltham, MA, United States) and used at 2 µg/ml for indirect immunofluorescence microscopy.

pUbC-LoxP-LaNtα31-T2A-tdTomato

A gBlock was synthesised (Integrated DNA Technologies, Coralville, IA) containing *Nde*I and *Nde*I restriction enzyme sites, T7 promoter binding site [41], Kozak consensus sequence [42], Igκ secretion signal (METDTLLLWVLLLWVPGSTGD) [43], LaNt α31-

352 encoding cDNA (amino acids 38-488) [25], Flag (DYKDDDDK) [44] and HA
353 (YPYDVPDYA) [45] tag sequences, T2A sequence (EGRGSLLTCGDVEENPGP) [46], and
354 *BamH*I. The gBlock DNA was inserted into pCSCMV:tdTomato (a gift from Gerhart Ryffel,
355 Addgene plasmid #30530 ; http://n2t.net/addgene:30530; RRID:Addgene_30530) using *Nde*I
356 and *BamH*I (New England Biolabs, Ipswich, MA), to produce pCS-LaNtα31-T2A-tdTomato.
357 LaNtα31-T2A-tdTomato was then removed from this backbone using *Nhe*I and *EcoR*I, and
358 inserted into a vector containing the Ubiquitin C (UbC) promoter and a floxed stop cassette,
359 all flanked by cHS4 insulator elements, producing pUbC-LoxP-LaNtα31-T2A-tdTomato.
360
361 **hK14-LaNt α31**
362 Full length LaNt α31 cDNA was amplified by PCR and inserted into pSecTag vector
363 (Thermo Fisher Scientific), introducing Igκ leader sequence 5' of the LaNt α31 sequence, and
364 Myc and 6x His tags 3' of the LaNt α31 sequence. The complete Igκ-LaNt α31-Myc-His
365 sequence was inserted into pGEM®-5Zf(+) vector (Promega, Madison, WI) using *Nhe*I and
366 *Pme*I (New England Biolabs), producing pGEM®-5Zf(+)-LaNt α31. Separately, the
367 sequence encoding human keratin 14 (hk14) promoter was amplified by PCR, using primers
368 introducing *Mlu*I 5' and *Nde*I, *Nsi*I 3' of the sequence, and this was inserted into a bicistronic
369 vector containing the mCherry seqeunce, producing phK14-mCherry. Finally, Igκ-LaNtα31-
370 Myc-His was excised from pGEM®-5Zf(+)-LaNtα31 using *Nde*I and *Nsi*I (New England
371 Biolabs) and inserted into phK14-mCherry, to produce phK14-LaNtα31-T2A-mCherry.
372
373 **Cloning procedures**
374 Restriction digests were set up with 1 μg of plasmid DNA, 1 μg of PCR product, or
375 100 ng of gBlock DNA, 20 U of each enzyme and CutSmart buffer (50 mM Potassium
376 Acetate, 20 mM Tris-acetate, 10 mM magnesium acetate, 100 μg/ml BSA (New England

377 Biolabs) and incubated at 37°C for 1 h. Enzymatic activity was inactivated by 20 min
378 incubation at 65°C. PCR or cloning products were separated using 1 % (w/v) agarose gels
379 (Thermo Fisher Scientific) dissolved in 1 x TAE electrophoresis buffer (40 mM Tris pH 7.6,
380 20 mM acetic acid, 1 mM EDTA) containing ethidium bromide, and visualised using a UV
381 transilluminator ChemiDoc MP System (BioRad, Hercules, CA). DNA bands of the correct
382 sizes were excised from the gel and purified using GenElute™ Gel Extraction Kit, following
383 manufacturer's protocol (Sigma Aldrich, St. Louis, Missouri, United States). Purified inserts
384 were ligated into vectors at 3:1 molar ratios, either using Instant Sticky-end Ligase Master
385 Mix (New England Biolabs) following manufacturers protocol, or using 400 U of T4 DNA
386 ligase and 1X reaction buffer (50 mM Tris-HCl, 10 mM $MgCl_2$ 1 mM ATP, 10 mM DTT,
387 New England Biolabs) at 16°C overnight, followed by enzymatic inactivation at 65°C for 10
388 min. Ligated DNA was heat-shock transformed into One-Shot TOP10 chemically competent
389 E. coli cells (Thermo Fisher Scientific) following manufacturer's protocol, then plated onto
390 LB plates containing the appropriate antibiotic (100 μg/ml ampicillin, 50 μg/ml kanamycin or
391 25 μg/ml chloramphenicol, Sigma Aldrich). Plasmid DNA was extracted from bacteria using
392 GenElute™ Plasmid Miniprep Kit (Sigma Aldrich), following the manufacturer's protocol.
393 Plasmids were sequenced by DNASeq (University of Dundee, Dundee, UK).
394
395 **Cell Culture**
396 KERA-308 murine epidermal keratinocyte cells [47], were purchased from CLS (Cell
397 Lines Service GmbH, Eppelheim, Germany) and maintained in high glucose (4.5 g/L)
398 Dulbecco's Modified Eagle Medium (DMEM, Sigma Aldrich) supplemented with 10% foetal
399 calf serum (LabTech, East Sussex, UK) and 2 mM L-glutamine (Sigma Aldrich). HEK293A
400 cells were maintained in DMEM supplemented with 10 % FCS and 4 mM L-glutamine.
401

Cell Transfections

1 x 10 KERA-308 or 4 x 10^5 HEK293A cells were seeded in 6-well plates (Greiner-BioOne, Kremsmünster, Austria) 24 h prior to transfection. For KERA-308 cells, 2 µg of hK14-LaNtα31-T2A-mCherry or LaNt-α31-pSec-Tag and 2 µl Lipofectamine 2000 (Thermo Fisher Scientific) were used. For HEK293A cells, either 1 µg pCAG-Cre:GFP and 2 µl Lipofectamine 2000, 2 µg of pUbC-LoxP-LaNtα31-T2A-tdTomato and 5 µl Lipofectamine 2000, or 2 µg of pUbC-LoxP-LaNtα31-T2A-tdTomato, 1 µg of pCAG-Cre:GFP and 7 µl Lipofectamine 2000 (Thermo Fisher Scientific), were mixed with 2 ml of Gibco™ Opti-MEM™ Reduced Serum Medium (Thermo Fisher Scientific) and incubated for 10 min at room temperature. The DNA-lipofectamine complex was added to the wells, and the media was replaced with DMEM high glucose after 6 h.

Explant culture method

Hair was removed from mouse skin tissue using Veet hair removal cream (Reckitt Benckiser, Slough, UK) and the skin washed in Dulbecco's Phosphate Buffered Saline (DPBS) containing 200 U/ml penicillin, 200 U/ml streptomycin, and 5 U/ml amphotericin B1 (all Sigma Aldrich). The skin was then dissected into 2-3 mm^2 pieces using a surgical scalpel and 3 or 4 pieces placed per well of a 6-well dish (Greiner Bio-One, Kremsmünster, Austria) with the dermis in contact with the dish. 300 µl of DMEM supplemented with 20% FCS, 2 mM L-glutamine, 200 µg/ml penicillin, 200 µg/ml streptomycin, and 5 µg/ml fungizone (all Sigma Aldrich) was added to the wells. After 24 h, each well was topped up with 1 ml of media, and the media was replenished every 48 h thereafter.

Transgenic Line establishment

Generation of transgenic mice were carried out based on the protocol described in [48]. C57Bl6CBAF1 females (Charles River Laboratories, Margate, Kent, UK) between 6-8 weeks were superovulated by intraperitoneal (IP) injections of 5 IU pregnant mare's serum gonadotrophin (PMSG; in 100µl H_2O), followed 46 h later by 5 IU of human chorionic gonadotropin (hCG, Sigma Aldrich). Treated females were mated with C57Bl6CBAF1 males overnight. Mated females were identified from the presence of copulation plugs, anaesthetised, and oviducts removed and dissected in M2 media (Millipore, Watford, UK). Day-1 oocytes (C57BL/6Jx CBA F1) were transferred into clean media by mouth pipetting. Cumulus cells were removed by hyaluronidase (300 µg/ml, Merck, Darmstadt, Germany) treatment in M2 media with gentle shaking until detached from the egg surface. Oocytes were then rinsed and transferred to M16 media (Millipore, Speciality Media, EmbryoMax) ready for injection.

DNA was diluted to a final concentration of 2 ng/µl in embryo water (Sigma Aldrich) and filter-purified using Durapore-PVDF 0.22 µM centrifuge filters (Merck). Injection pipettes were used to pierce the outer layers of the oocyte and to inject DNA. DNA was injected into the pronuclei of the oocyte. Undamaged eggs were transferred to clean M16 media and incubated at 37 °C until transferred into pseudopregnant CD1 females on the same day. Meanwhile, pseudopregnant females were obtained by mating vasectomised CD1 males overnight. Copulation plugs were checked and females were used 1 day post-coitum. Females were anaesthetised by inhalation of isoflurane (Sigma Aldrich). 30 injected oocytes were transferred to plugged pseudopregnant female oviducts through the infundibulum.

In generating the pUbC-LoxP-LaNtα31-T2A-tdTomato line, 460 mouse zygotes were injected over four sessions. 87% of these zygotes survived and were transferred into 11 recipient CD1 mothers. From these mothers, 42 pups were born. Of the 10 F0 mice that gave

a positive genotype result, four passed on the transgene to the F1 generation. Mice that did not pass on the transgene to the F1 generation were culled, the four F0 mice were mated to expand colonies for cryopreservation, and one line was continued for investigation.

For K14-LaNtα31 transgenic mice, 140 embryos were transferred into five recipient CD1 mothers. Three small litters were born, totalling seven pups. two pups possessed the transgene, and these were mated to generate F1 mice.

R26CreERT2 (Jax Lab 008463) [49] mice were purchased from The Jackson Laboratory (Bar Harbor, Maine, United States).

In Vivo Transgene Induction

Tamoxifen (Sigma Aldrich) was dissolved in corn oil (Sigma Aldrich) and administered via IP at a concentrations of 25 mg/kg or 75 mg/kg. Progesterone (Sigma Aldrich) was dissolved in corn oil (Sigma Aldrich) and was co-administered alongside tamoxifen at a dose of exactly half of the corresponding tamoxifen dose (12.5 mg/kg or 25 mg/kg).

DNA Extraction

Four weeks after birth, ear notches were collected from mouse pups and digested in 100 µl lysis buffer (50 mM Tris-HCl pH 8.0, 0.1 M NaCl, 1% SDS, 20 mM EDTA) and 10 µl of proteinase K (10 mg/ml, all Sigma Aldrich) overnight at 55°C. The following day, samples were cooled, spun at 13,000 rpm for 3 min and the supernatant transferred to clean 1.5 ml tubes (Eppendorf, Hamburg, Germany). An equal volume of isopropanol (Sigma Aldrich) was added, gently inverted and span at 13,000 rpm, and supernatant discarded. Pellets were washed with 500 µl of 70 % EtOH (Sigma Aldrich), then air-dried for 10 min, and resuspended in 50 µl ddH_20.

PCR

50 ng of genomic DNA was mixed with 12.5 µl of REDtaq ReadyMix PCR Reaction Mix (20 mM Tris-HCl pH 8.3, 100 mM KCl, 3 mM MgCl2, 0.002 % gelatin, 0.4 mM dNTP mix, 0.06 unit/ml of Taq DNA Polymerase, Sigma Aldrich) and 0.5 µM of each primer; ddH_20 was added to make the reaction mixture up to 25 µl. Primer pairs for genotyping were as follows: LaNt α31 to tdTomato Forward 5' –ATCTATGCTGGTGGAGGGGT – 3', Reverse 5' – TCTTTGATGACCTCCTCGCC – 3'; Cre Forward 5' – GCATTACCGGTCGATGCAACGAGTGATGAG – 3', Reverse 5' – GAGTGAACGAACCTGGTCGAAATCAGTGCG – 3'; Recombination Forward 5' – TCCGCTAAATTCTGGCCGTT – 3', Reverse 5' – GTGCTTTCCTGGGGTCTTCA – 3'(all from Integrated DNA Technologies). Cycle conditions were as follows: Genotyping – 1 cycle of 95 °C for 5 min, 35 cycles of 95 °C for 15 s; 56 °C for 30 s; 72 °C for 40 s, followed by a final cycle of 72 °C for 5 min. For checking recombination: 1 cycle of 95 °C for 5 min, 35 cycles of 95 °C for 15 s; 60 °C for 30 s; 72 °C for 90 s, followed by a final cycle of 72 °C for 7 min. PCR products were separated by gel electrophoresis and imaged using a BioRad Gel Doc XR+ System.

SDS-PAGE and western immunoblotting

Cells were homogenized by scraping into 90 µL Urea/SDS buffer: 10 mM Tris-HCl pH 6.8, 6.7 M urea, 1 % w/v SDS, 10 % v/v glycerol and 7.4 µM bromophenol blue, containing 50 µM phenylmethysulfonyl fluoride (PMSF) and 50 µM N-methylmaleimide (all Sigma Aldrich). Lysates were sonicated and 10 % v/v β-mercaptoethanol (Sigma Aldrich) added. Proteins were separated by sodium dodecyl sulfate-polyacrylamide gel electrophoresis (SDS-PAGE) using 10 % polyacrylamide gels; 1.5 M Tris, 0.4 % w/v SDS, 10 % acrylamide/

bis-acrylamide (all Sigma Aldrich), electrophoresis buffer; 25 mM tris-HCl, 190 mM glycine, 0.1 % w/v SDS, pH 8.5 (all Sigma Aldrich). Proteins were transferred to a nitrocellulose membrane using the TurboBlot™ system (BioRad) and blocked at room temperature in Odyssey® TBS-Blocking Buffer (Li-Cor BioSciences, Lincoln, NE, United States) for 1 h. The membranes were probed overnight at 4 °C diluted in blocking buffer, washed 3 x 5 min in PBS with 0.1 % Tween (both Sigma Aldrich) and probed for 1 h at room temperature in the dark with IRDye® conjugated secondary Abs against goat IgG (800CW) and rabbit IgG (680CW), raised in goat or donkey (LiCor BioSciences), diluted in Odyssey® TBS-Blocking Buffer at 0.05 µg/ml. Membranes were then washed for 3 x 5 min in PBS with 0.1 % Tween, rinsed with ddH_2O and imaged using the Odyssey® CLX 9120 infrared imaging system (LiCor BioSciences). Image Studio Light v.5.2 was used to process scanned membranes.

Tissue processing

For cryosections, P0 pups were culled by cervical dislocation, and fixed in 4 % paraformaldehyde (Merck) overnight at 4 °C. Samples were cryoprotected in 30 % sucrose/PBS solutions then in 30 % sucrose/PBS:O.C.T (1:1) solutions (Tissue-Tek, Sakura Finetek Europe, Alphen aan den Rijn, The Netherlands), each overnight at 4 °C. Samples were embedded in OCT compound and transferred on dry ice. Embedded samples were sectioned at 8 µm using a Leica CM1850 cryostat (Leica, Wokingham, UK). For paraffin sections, Tissues were fixed in 10 % neutral buffered formalin (Leica,) for 24 h, then processed through graded ethanol and xylene before being embedded in paraffin wax. 5 µm sections were cut using a rotary microtome RM2235 (Leica), adhered to microscope slides, then dried overnight at 37 °C. Sections were dewaxed and rehydrated with xylene followed by a series of decreasing ethanol concentrations. Antigen retrieval was performed by microwaving sections in preheated 0.01 M citrate buffer pH 6 (Sigma Aldrich) for 5 min.

525

526 **Hematoxylin and Eosin Staining**

527 Sections were dewaxed and rehydrated with xylene followed by a series of decreasing
528 ethanol concentrations. Sections were then stained in Harris hematoxylin solution (Leica) for
529 5 min, H_2O for 1 min, acid alcohol (Leica) for 5 s, H_2O for 5 min, aqueous eosin (Leica) for 3
530 min, H_2O for 15 s, followed by dehydration through graded ethanol and xylene. Slides were
531 coverslipped with DPX mounting media (Sigma Aldrich).

532

533 **Immunohistochemistry**

534 Slides were incubated in ice-cold acetone for 10 min, then transferred into PBS for 10
535 minblocking, then blocked in PBS containing 10 % normal goat serum (NGS) at room
536 temperature for 1 h. Next, samples were probed with the primary antibodies diluted in PBS-
537 Tween (0.05 %) with 5 % NGS at 4 °C overnight. Samples were then washed for 3 x 5 min in
538 PBS-Tween (0.05 %), before being probed with secondary antibodies diluted in PBS-Tween
539 (0.05%) with 5 % NGS at room temperature for 1 h. Samples were washed for 3 x 5 min in
540 PBS-Tween (0.05 %). Slides were mounted with VECTASHIELD® Antifade Mounting
541 Medium with DAPI (VECTASHIELD®, Burlingame, CA).

542

543 **Image Acquisition**

544 H&E images were acquired using a Zeiss Axio Scan.Z1 equipped with an Axiocam
545 colour CCD camera using ZEN Blue software (all from Zeiss, Oberkochen, Germany). Live
546 cell images were acquired using a Nikon Eclipse Ti-E microscope (Nikon, Tokyo, Japan).
547 Immunofluorescence images of tissues were acquired using a Zeiss LSM 800 confocal
548 microscope (Zeiss).

549

Image Analysis

Images were processed using either Zen 2.6 (blue edition) (Zeiss) or ImageJ (National Institutes of Health, Bethesda, MD, United States)[50]. Stardist plugin [51] was used for segmentation of nuclei from H&E images. Images were thresholded manually to remove areas containing no tissue in the images.

Acknowledgements

We are grateful to the staff at the University of Liverpool Biomedical Services Unit. We would like to thank Dr. Takao Sakai, Dr. Rachel Lennon, and Dr. Mychel Morais for helpful discussions during the writing of this manuscript.

Author contributions:

Conor J. Sugden: Methodology, Validation, Formal analysis, Investigation, Data Curation, Writing - Original Draft, Writing - Review & Editing, Visualization. **Valentina Iorio:** Methodology, Investigation, Data Curation, Writing - Review & Editing. **Lee D. Troughton:** Methodology, Writing - Original Draft, Writing - Review & Editing. **Ke Liu:** Methodology, Writing - Review & Editing. **George Bou-Gharios:** Conceptualization, Methodology, Writing - Review & Editing, Supervision. **Kevin Hamill:** Conceptualization, Methodology, Writing - Original Draft , Writing - Review & Editing, Supervision, Funding acquisition.

Funding:

This work was supported by the biotechnology and biological sciences research council [grant number BB/L020513/1] and the The University of Liverpool Crossley Barnes Bequest fund.

References

1. Yamada, K.M., et al., *Extracellular matrix dynamics in cell migration, invasion and tissue morphogenesis.* Int J Exp Pathol, 2019. **100**(3): p. 144-152.
2. Sekiguchi, R. and K.M. Yamada, *Basement Membranes in Development and Disease*. Curr Top Dev Biol, 2018. **130**: p. 143-191.
3. Yurchenco, P.D., *Basement membranes: cell scaffoldings and signaling platforms.* Cold Spring Harb Perspect Biol, 2011. **3**(2).
4. Pozzi, A., P.D. Yurchenco, and R.V. Iozzo, *The nature and biology of basement membranes.* Matrix Biol, 2017. **57-58**: p. 1-11.
5. Walma, D.A.C. and K.M. Yamada, *The extracellular matrix in development.* Development, 2020. **147**(10).
6. Morrissey, M.A. and D.R. Sherwood, *An active role for basement membrane assembly and modification in tissue sculpting.* J Cell Sci, 2015. **128**(9): p. 1661-8.
7. Theocharis, A.D., et al., *Extracellular matrix structure.* Adv Drug Deliv Rev, 2016. **97**: p. 4-27.
8. Hamill, K.J., et al., *Laminin deposition in the extracellular matrix: a complex picture emerges.* J Cell Sci, 2009. **122**(Pt 24): p. 4409-17.
9. Hohenester, E. and P.D. Yurchenco, *Laminins in basement membrane assembly.* Cell Adh Migr, 2013. **7**(1): p. 56-63.
10. Aumailley, M., *The laminin family.* Cell Adh Migr, 2013. **7**(1): p. 48-55.
11. Aumailley, M., et al., *A simplified laminin nomenclature.* Matrix Biol, 2005. **24**(5): p. 326-32.
12. Cheng, Y.S., et al., *Self-assembly of laminin isoforms.* J Biol Chem, 1997. **272**(50): p. 31525-32.
13. Odenthal, U., et al., *Molecular analysis of laminin N-terminal domains mediating self-interactions.* J Biol Chem, 2004. **279**(43): p. 44504-12.
14. Schittny, J.C. and P.D. Yurchenco, *Terminal short arm domains of basement membrane laminin are critical for its self-assembly.* J Cell Biol, 1990. **110**(3): p. 825-32.
15. Yurchenco, P.D. and Y.S. Cheng, *Laminin self-assembly: a three-arm interaction hypothesis for the formation of a network in basement membranes.* Contrib Nephrol, 1994. **107**: p. 47-56.
16. Purvis, A. and E. Hohenester, *Laminin network formation studied by reconstitution of ternary nodes in solution.* J Biol Chem, 2012. **287**(53): p. 44270-7.
17. Carafoli, F., S.A. Hussain, and E. Hohenester, *Crystal structures of the network-forming short-arm tips of the laminin beta1 and gamma1 chains.* PLoS One, 2012. **7**(7): p. e42473.

18. McKee, K.K., M. Aleksandrova, and P.D. Yurchenco, *Chimeric protein identification of dystrophic, Pierson and other laminin polymerization residues.* Matrix Biol, 2018. **67**: p. 32-46.
19. Matejas, V., et al., *Mutations in the human laminin beta2 (LAMB2) gene and the associated phenotypic spectrum.* Hum Mutat, 2010. **31**(9): p. 992-1002.
20. Funk, S.D., M.H. Lin, and J.H. Miner, *Alport syndrome and Pierson syndrome: Diseases of the glomerular basement membrane.* Matrix Biol, 2018. **71-72**: p. 250-261.
21. Gawlik, K.I. and M. Durbeej, *Skeletal muscle laminin and MDC1A: pathogenesis and treatment strategies.* Skelet Muscle, 2011. **1**(1): p. 9.
22. Funk, S.D., et al., *Pathogenicity of a Human Laminin beta2 Mutation Revealed in Models of Alport Syndrome.* J Am Soc Nephrol, 2018. **29**(3): p. 949-960.
23. Hohenester, E., *Structural biology of laminins.* Essays Biochem, 2019. **63**(3): p. 285-295.
24. Yousif, L.F., J. Di Russo, and L. Sorokin, *Laminin isoforms in endothelial and perivascular basement membranes.* Cell Adh Migr, 2013. **7**(1): p. 101-10.
25. Hamill, K.J., et al., *Identification of a novel family of laminin N-terminal alternate splice isoforms: structural and functional characterization.* J Biol Chem, 2009. **284**(51): p. 35588-96.
26. Rajasekharan, S. and T.E. Kennedy, *The netrin protein family.* Genome Biol, 2009. **10**(9): p. 239.
27. Ettner, N., et al., *The N-terminal globular domain of the laminin alpha1 chain binds to alpha1beta1 and alpha2beta1 integrins and to the heparan sulfate-containing domains of perlecan.* FEBS Lett, 1998. **430**(3): p. 217-21.
28. Horejs, C.M., et al., *Biologically-active laminin-111 fragment that modulates the epithelial-to-mesenchymal transition in embryonic stem cells.* Proc Natl Acad Sci U S A, 2014. **111**(16): p. 5908-13.
29. Kariya, Y., et al., *Characterization of laminin 5B and NH2-terminal proteolytic fragment of its alpha3B chain: promotion of cellular adhesion, migration, and proliferation.* J Biol Chem, 2004. **279**(23): p. 24774-84.
30. Lai Wing Sun, K., J.P. Correia, and T.E. Kennedy, *Netrins: versatile extracellular cues with diverse functions.* Development, 2011. **138**(11): p. 2153-69.
31. Fahey, B. and B.M. Degnan, *Origin and evolution of laminin gene family diversity.* Mol Biol Evol, 2012. **29**(7): p. 1823-36.
32. Leclere, L. and F. Rentzsch, *Repeated evolution of identical domain architecture in metazoan netrin domain-containing proteins.* Genome Biol Evol, 2012. **4**(9): p. 883-99.

33. Reuten, R., et al., *Structural decoding of netrin-4 reveals a regulatory function towards mature basement membranes.* Nat Commun, 2016. **7**: p. 13515.
34. Schneiders, F.I., et al., *Binding of netrin-4 to laminin short arms regulates basement membrane assembly.* J Biol Chem, 2007. **282**(33): p. 23750-8.
35. Larrieu-Lahargue, F., et al., *Netrin-4 induces lymphangiogenesis in vivo.* Blood, 2010. **115**(26): p. 5418-26.
36. Koch, M., et al., *A novel member of the netrin family, beta-netrin, shares homology with the beta chain of laminin: identification, expression, and functional characterization.* J Cell Biol, 2000. **151**(2): p. 221-34.
37. Barrera, V., et al., *Differential Distribution of Laminin N-Terminus alpha31 Across the Ocular Surface: Implications for Corneal Wound Repair.* Invest Ophthalmol Vis Sci, 2018. **59**(10): p. 4082-4093.
38. Troughton, L.D., et al., *Laminin N-terminus α31 protein distribution in adult human tissues.* bioRxiv, 2020: p. 2020.05.21.108134.
39. Troughton, L.D., T. Zech, and K.J. Hamill, *Laminin N-terminus α31 is upregulated in invasive ductal breast cancer and changes the mode of tumour invasion.* bioRxiv, 2020: p. 2020.05.28.120964.
40. Iorio, V., et al., *LaNt α31 modulates LM332 organisation during matrix deposition leading to cell-matrix adhesion and migration defects.* bioRxiv, 2019: p. 617597.
41. Pribnow, D., *Nucleotide sequence of an RNA polymerase binding site at an early T7 promoter.* Proc Natl Acad Sci U S A, 1975. **72**(3): p. 784-8.
42. Kozak, M., *An analysis of 5'-noncoding sequences from 699 vertebrate messenger RNAs.* Nucleic Acids Res, 1987. **15**(20): p. 8125-48.
43. Coloma, M.J., et al., *Novel vectors for the expression of antibody molecules using variable regions generated by polymerase chain reaction.* J Immunol Methods, 1992. **152**(1): p. 89-104.
44. Brizzard, B.L., R.G. Chubet, and D.L. Vizard, *Immunoaffinity purification of FLAG epitope-tagged bacterial alkaline phosphatase using a novel monoclonal antibody and peptide elution.* Biotechniques, 1994. **16**(4): p. 730-5.
45. Field, J., et al., *Purification of a RAS-responsive adenylyl cyclase complex from Saccharomyces cerevisiae by use of an epitope addition method.* Mol Cell Biol, 1988. **8**(5): p. 2159-65.
46. Kim, J.H., et al., *High cleavage efficiency of a 2A peptide derived from porcine teschovirus-1 in human cell lines, zebrafish and mice.* PLoS One, 2011. **6**(4): p. e18556.
47. Yuspa, S.H. and C.C. Harris, *Altered differentiation of mouse epidermal cells treated with retinyl acetate in vitro.* Exp Cell Res, 1974. **86**(1): p. 95-105.

48. Ittner, L.M. and J. Gotz, *Pronuclear injection for the production of transgenic mice.* Nat Protoc, 2007. **2**(5): p. 1206-15.
49. Ventura, A., et al., *Restoration of p53 function leads to tumour regression in vivo.* Nature, 2007. **445**(7128): p. 661-5.
50. Schneider, C.A., W.S. Rasband, and K.W. Eliceiri, *NIH Image to ImageJ: 25 years of image analysis.* Nat Methods, 2012. **9**(7): p. 671-5.
51. Schmidt, U., et al. *Cell Detection with Star-Convex Polygons*. 2018. Cham: Springer International Publishing.
52. Ochiai, H., H. Harashima, and H. Kamiya, *Effects of insulator cHS4 on transgene expression from plasmid DNA in a positive feedback system.* J Biosci Bioeng, 2011. **112**(5): p. 432-4.
53. Zenker, M., et al., *Human laminin beta2 deficiency causes congenital nephrosis with mesangial sclerosis and distinct eye abnormalities.* Hum Mol Genet, 2004. **13**(21): p. 2625-32.
54. Zenker, M., et al., *Demonstration of two novel LAMB2 mutations in the original Pierson syndrome family reported 42 years ago.* Am J Med Genet A, 2005. **138**(1): p. 73-4.
55. Hinkes, B.G., et al., *Nephrotic syndrome in the first year of life: two thirds of cases are caused by mutations in 4 genes (NPHS1, NPHS2, WT1, and LAMB2).* Pediatrics, 2007. **119**(4): p. e907-19.
56. Chen, Y.M., Y. Kikkawa, and J.H. Miner, *A missense LAMB2 mutation causes congenital nephrotic syndrome by impairing laminin secretion.* J Am Soc Nephrol, 2011. **22**(5): p. 849-58.
57. Kiritsi, D., C. Has, and L. Bruckner-Tuderman, *Laminin 332 in junctional epidermolysis bullosa.* Cell Adh Migr, 2013. **7**(1): p. 135-41.
58. McLean, W.H., et al., *An unusual N-terminal deletion of the laminin alpha3a isoform leads to the chronic granulation tissue disorder laryngo-onycho-cutaneous syndrome.* Hum Mol Genet, 2003. **12**(18): p. 2395-409.
59. Barzegar, M., et al., *A new homozygous nonsense mutation in LAMA3A underlying laryngo-onycho-cutaneous syndrome.* Br J Dermatol, 2013. **169**(6): p. 1353-6.
60. Pierce, R.A., et al., *Expression of laminin alpha3, alpha4, and alpha5 chains by alveolar epithelial cells and fibroblasts.* Am J Respir Cell Mol Biol, 1998. **19**(2): p. 237-44.
61. DeBiase, P.J., et al., *Laminin-311 (Laminin-6) fiber assembly by type I-like alveolar cells.* J Histochem Cytochem, 2006. **54**(6): p. 665-72.
62. Morales-Nebreda, L.I., et al., *Lung-specific loss of alpha3 laminin worsens bleomycin-induced pulmonary fibrosis.* Am J Respir Cell Mol Biol, 2015. **52**(4): p. 503-12.
63. Coulombe, P.A., R. Kopan, and E. Fuchs, *Expression of keratin K14 in the epidermis and hair follicle: insights into complex programs of differentiation.* J Cell Biol, 1989. **109**(5): p. 2295-312.

64. Vasioukhin, V., et al., *The magical touch: genome targeting in epidermal stem cells induced by tamoxifen application to mouse skin.* Proc Natl Acad Sci U S A, 1999. **96**(15): p. 8551-6.
65. Wang, X., et al., *Transgenic studies with a keratin promoter-driven growth hormone transgene: prospects for gene therapy.* Proc Natl Acad Sci U S A, 1997. **94**(1): p. 219-26.
66. Hafner, M., et al., *Keratin 14 Cre transgenic mice authenticate keratin 14 as an oocyte-expressed protein.* Genesis, 2004. **38**(4): p. 176-81.
67. Hussain, S.A., F. Carafoli, and E. Hohenester, *Determinants of laminin polymerization revealed by the structure of the alpha5 chain amino-terminal region.* EMBO Rep, 2011. **12**(3): p. 276-82.
68. Jones, L.K., et al., *A mutation affecting laminin alpha 5 polymerisation gives rise to a syndromic developmental disorder.* Development, 2020.
69. Noakes, P.G., et al., *Aberrant differentiation of neuromuscular junctions in mice lacking s-laminin/laminin beta 2.* Nature, 1995. **374**(6519): p. 258-62.
70. Noakes, P.G., et al., *The renal glomerulus of mice lacking s-laminin/laminin beta 2: nephrosis despite molecular compensation by laminin beta 1.* Nat Genet, 1995. **10**(4): p. 400-6.
71. Miner, J.H., et al., *Transgenic isolation of skeletal muscle and kidney defects in laminin beta2 mutant mice: implications for Pierson syndrome.* Development, 2006. **133**(5): p. 967-75.
72. Jarad, G., et al., *Proteinuria precedes podocyte abnormalities inLamb2-/- mice, implicating the glomerular basement membrane as an albumin barrier.* J Clin Invest, 2006. **116**(8): p. 2272-9.
73. Libby, R.T., et al., *Disruption of laminin beta2 chain production causes alterations in morphology and function in the CNS.* J Neurosci, 1999. **19**(21): p. 9399-411.
74. Denes, V., et al., *Laminin deficits induce alterations in the development of dopaminergic neurons in the mouse retina.* Vis Neurosci, 2007. **24**(4): p. 549-62.
75. Hallmann, R., et al., *Expression and function of laminins in the embryonic and mature vasculature.* Physiol Rev, 2005. **85**(3): p. 979-1000.
76. Petajaniemi, N., et al., *Localization of laminin alpha4-chain in developing and adult human tissues.* J Histochem Cytochem, 2002. **50**(8): p. 1113-30.
77. Vainionpaa, N., et al., *Basement membrane protein distribution in LYVE-1-immunoreactive lymphatic vessels of normal tissues and ovarian carcinomas.* Cell Tissue Res, 2007. **328**(2): p. 317-28.
78. Moore, M.A. and D. Metcalf, *Ontogeny of the haemopoietic system: yolk sac origin of in vivo and in vitro colony forming cells in the developing mouse embryo.* Br J Haematol, 1970. **18**(3): p. 279-96.

79. Sanchez, M.J., et al., *Characterization of the first definitive hematopoietic stem cells in the AGM and liver of the mouse embryo.* Immunity, 1996. **5**(6): p. 513-25.
80. Dzierzak, E. and N.A. Speck, *Of lineage and legacy: the development of mammalian hematopoietic stem cells.* Nat Immunol, 2008. **9**(2): p. 129-36.
81. Qian, H., et al., *Contribution of alpha6 integrins to hematopoietic stem and progenitor cell homing to bone marrow and collaboration with alpha4 integrins.* Blood, 2006. **107**(9): p. 3503-10.
82. Potocnik, A.J., C. Brakebusch, and R. Fassler, *Fetal and adult hematopoietic stem cells require beta1 integrin function for colonizing fetal liver, spleen, and bone marrow.* Immunity, 2000. **12**(6): p. 653-63.
83. Hirsch, E., et al., *Impaired migration but not differentiation of haematopoietic stem cells in the absence of beta1 integrins.* Nature, 1996. **380**(6570): p. 171-5.
84. Staquicini, F.I., et al., *Discovery of a functional protein complex of netrin-4, laminin gamma1 chain, and integrin alpha6beta1 in mouse neural stem cells.* Proc Natl Acad Sci U S A, 2009. **106**(8): p. 2903-8.
85. Sher, I., et al., *Targeting perlecan in human keratinocytes reveals novel roles for perlecan in epidermal formation.* J Biol Chem, 2006. **281**(8): p. 5178-87.
86. Penton, C.M., et al., *Laminin 521 maintains differentiation potential of mouse and human satellite cell-derived myoblasts during long-term culture expansion.* Skelet Muscle, 2016. **6**(1): p. 44.
87. Kiyozumi, D., et al., *Laminin is the ECM niche for trophoblast stem cells.* Life Sci Alliance, 2020. **3**(2).
88. Rodin, S., et al., *Long-term self-renewal of human pluripotent stem cells on human recombinant laminin-511.* Nat Biotechnol, 2010. **28**(6): p. 611-5.
89. Polisetti, N., et al., *Laminin-511 and -521-based matrices for efficient ex vivo-expansion of human limbal epithelial progenitor cells.* Sci Rep, 2017. **7**(1): p. 5152.
90. Sunada, Y., et al., *Identification of a novel mutant transcript of laminin alpha 2 chain gene responsible for muscular dystrophy and dysmyelination in dy2J mice.* Hum Mol Genet, 1995. **4**(6): p. 1055-61.
91. Xu, H., et al., *Murine muscular dystrophy caused by a mutation in the laminin alpha 2 (Lama2) gene.* Nat Genet, 1994. **8**(3): p. 297-302.
92. Payne, S., S. De Val, and A. Neal, *Endothelial-Specific Cre Mouse Models.* Arterioscler Thromb Vasc Biol, 2018. **38**(11): p. 2550-2561.
93. Poulos, M.G., et al., *Developments in RNA splicing and disease.* Cold Spring Harb Perspect Biol, 2011. **3**(1): p. a000778.

829 94. Baralle, F.E. and J. Giudice, *Alternative splicing as a regulator of*
830 *development and tissue identity.* Nat Rev Mol Cell Biol, 2017. **18**(7): p.
831 437-451.
832 95. Ffrench-Constant, C., et al., *Reappearance of an embryonic pattern of*
833 *fibronectin splicing during wound healing in the adult rat.* J Cell Biol,
834 1989. **109**(2): p. 903-14.
835

Figure legends

Figure 1 - Validation of UbCLaNt Cre-inducible construct in vitro

A) Diagram of the pUbC-LoxP-LaNt-α31-T2A-tdTomato construct. B) HEK 293A cells were transfected with pUbC-LoxP-LaNt-α31-T2A-tdTomato, pCAG-Cre:GFP, or pUbC-LoxP-LaNt-α31-T2A-tdTomato and pCAG-Cre:GFP and imaged 48 h after transfection. Scale bar 100 µm C) PCR was performed using primers flanking the stop cassette on DNA extracted from HEK293A cells co-transfected with pUbC-LoxP-LaNt-α31-T2A-tdTomato and pCAG-Cre:GFP. D) Western blot of lysates from HEK293 cells either untransfected or transfected with CMV- LaNt-α31-T2A-Dendra2 (positive control), or pUbC-LoxP-LaNt-α31-T2A-tdTomato and pCAG-Cre:GFP then probed with anti-flag antibodies

Figure 2 -UbC-LoxP-LaNt-α31-T2A-tdTomato embryonic fibroblast express the transgene upon transduction with a Cre recombinase-coding adenovirus

A) PCR was performed on gDNA of F1 UbC-LoxP-LaNt-α31-T2A-tdTomato embryos. B) Western blot of protein lysates from explanted F1 mouse embryonic fibroblasts processed with anti-HA antibodies. C) Fluorescence microscopy images of explanted cells from UbC-LoxP-LaNt-α31-T2A-tdTomato F1 mice. Scale bar = 100 µm.

Figure 3 - UbCLaNtα31 x R26CreERT2 ER transgenic mice express the UbC-LaNtα31 transgene following exposure to tamoxifen

A) Schematic diagram of the UbC-LaNt-α31 and Rosa-Cre transgenes. B) PCR performed using primers flanking the stop cassette on DNA extracted from transgenic mouse embryos from a UbCLaNtα31 x R26CreERT2 mating. C) Phase contrast and fluorescence microscopy images of explanted cells from UbCLaNtα31::R26CreERT2 embryos. Scale bar = 100 µm.

D) Western blot of lysates from UbCLaNtα31::R26CreERT2 embryo explants processed with anti-HA antibodies.

Figure 4 - Transgenic mice overexpressing LaNtα31 display localised regions of erythema

A) Representative images of UbCLaNt::R26CreERT2 P0 mice B) PCR genotyping of transgenic mice. C) Fluorescence microscopy images of explanted cells from UbCLaNt::R26CreERT2 P0 mice. D) Western blot of tissue lysates of UbCLaNt::R26CreERT2 P0 mice. E) Representative fluorescence microscopy UbCLaNt::R26CreERT2 P0 mouse OCT sections (8 μm) probed with anti-mCherry antibodies. Yellow arrows indicate cells expressing the tdTomato transgene reporter. Scale bar = 100 μm.

Figure 5 - LaNt α31 overexpression leads to epithelial detachment, tubular dilation and interstitial bleeding in the kidney.

Representative images of H&E stained FFPE sections (5 μm) of newborn UbCLaNt::R26CreERT2 transgenic mouse kidneys. Middle and right columns show areas of increased magnification. Black arrows point to areas of epithelial detachment. White arrows point to tubular dilation. Yellow arrows point to areas of interstitial bleeding. Scale bar = 100 μm.

Figure 6 - LaNt α31 overexpression causes a thickening of the tubular basement membrane.

UbCLaNt::R26CreERT2 P0 mouse FFPE sections (5 μm) processed for immunohistochemistry with anti-laminin 111 polyclonal antibodies. Middle and right columns show areas of increased magnification. Scale bars = 100 μm.

Figure 7 - LaNt α31 overexpression disrupts epidermal-dermal basement membrane.

A) H&E staining of FFPE sections (5 μm) of newborn UbCLaNt::R26CreERT2 transgenic mouse dorsal skin. Middle and right columns show increased magnification of the epithelium or hair follicles respectively. Yellow arrows indicate basal layer of epithelial cells. Scale bar = 100 μm. B) UbCLaNt::R26CreERT2 P0 mouse FFPE sections (5 μm) processed for immunohistochemistry with anti-laminin 111 immunoreactivity. Middle and right columns show areas of increased magnification. Yellow arrows indicate the epidermal-dermal junction. Scale bar = 100 μm.

Figure 8 - Mice expressing the LaNtα31 transgene display structural differences in the lung.

UbCLaNtα31::R26CreERT2 P0 lung FFPE sections (5 μm) stained with H&E. Middle and right columns show areas of increased magnification. Scale bar = 100 μm.

Figure 9 - LaNt α31 overexpression leads to a reduction of hematopoietic colonies in the liver

A) H&E staining of FFPE sections (5 μm) of newborn UbCLaNt::R26CreERT2 transgenic mouse skin. Middle and right columns show increased magnification of different area of the liver. Yellow arrowheads highlight areas of increased cell density. Scale bar =

100 μm. B) Representative image analysis method of determining nuclei count. C) Quantification of nuclei.

Supplemental figure 1 – Transgenic expression of LaNt α31 under control of the human keratin-14 promoter results in a low number of offspring.

A) Diagram of the phK14-LaNtα31-T2A-mCherry construct. B) Fluorescence microscopy images of KERA 308 cells transfected with phK14-LaNtα31-T2A-mCherry. C) Western blot of protein lysates from transfected KERA 308 cells. D) Schematic of F0 mice generation and PCR genotyping of F0 mice. E) PCR genotyping of F1 mice. F) Representative fluorescence images of frozen sections from F1 mice tissues. G) Western blot of tissue lysates from F1 mice, probed with anti-His antibodies.

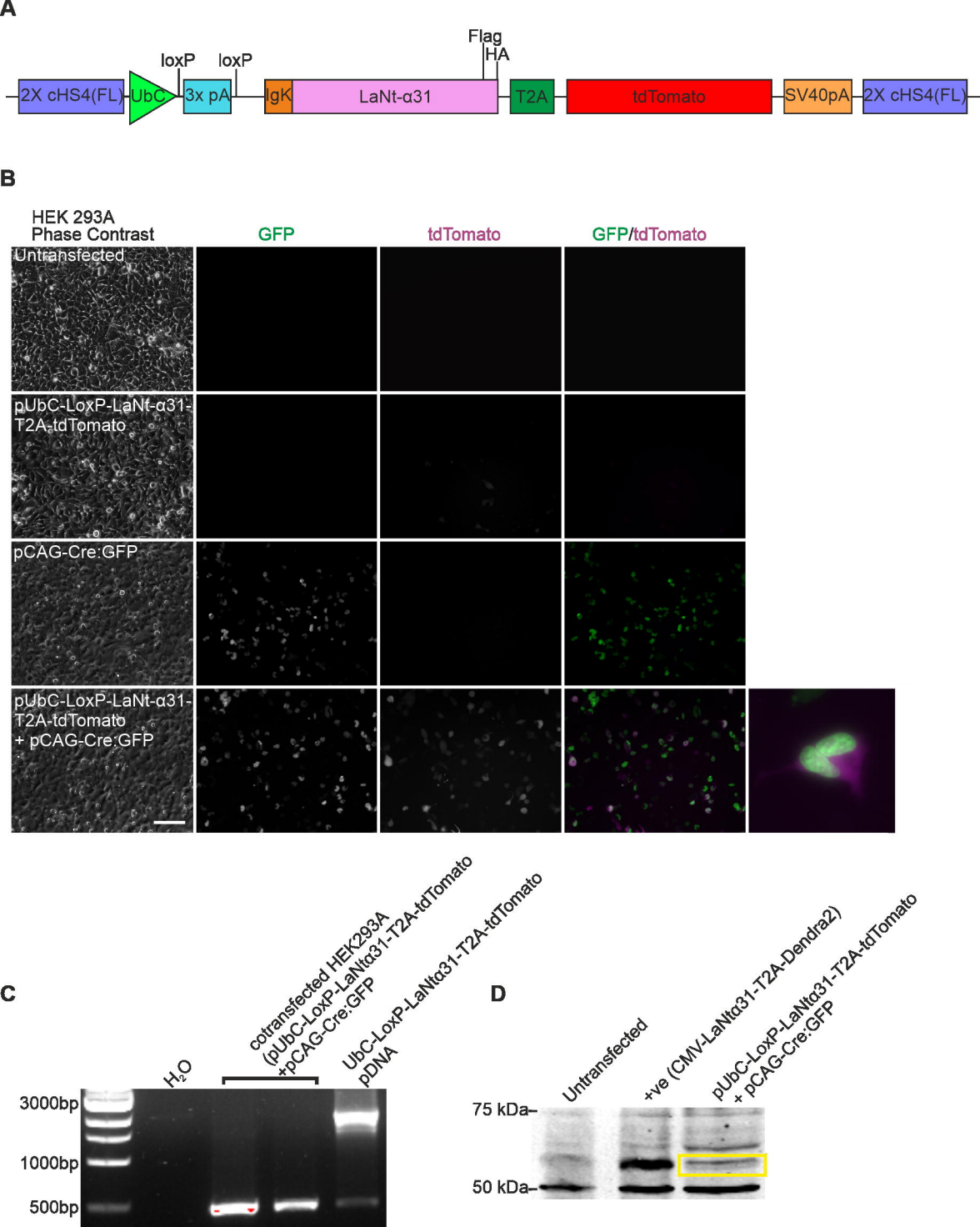
A
loxP
loxP
Flag
HA
2X cHS4(FL)
UbC
3x pA
IgK
LaNt-α31
T2A
tdTomato
SV40pA
2X cHS4(FL)
B
HEK 293A
Phase Contrast
GFP
tdTomato
GFP/tdTomato
Untransfected
pUbC-LoxP-LaNt-α31-T2A-tdTomato
pCAG-Cre:GFP
pUbC-LoxP-LaNt-α31-T2A-tdTomato + pCAG-Cre:GFP
C
H2O
cotransfected HEK293A (pUbC-LoxP-LaNtα31-T2A-tdTomato +pCAG-Cre:GFP
UbC-LoxP-LaNtα31-T2A-tdTomato pDNA
3000bp
1000bp
500bp
D
Untransfected
+ve (CMV-LaNtα31-T2A-Dendra2)
pUbC-LoxP-LaNtα31-T2A-tdTomato + pCAG-Cre:GFP
75 kDa
50 kDa

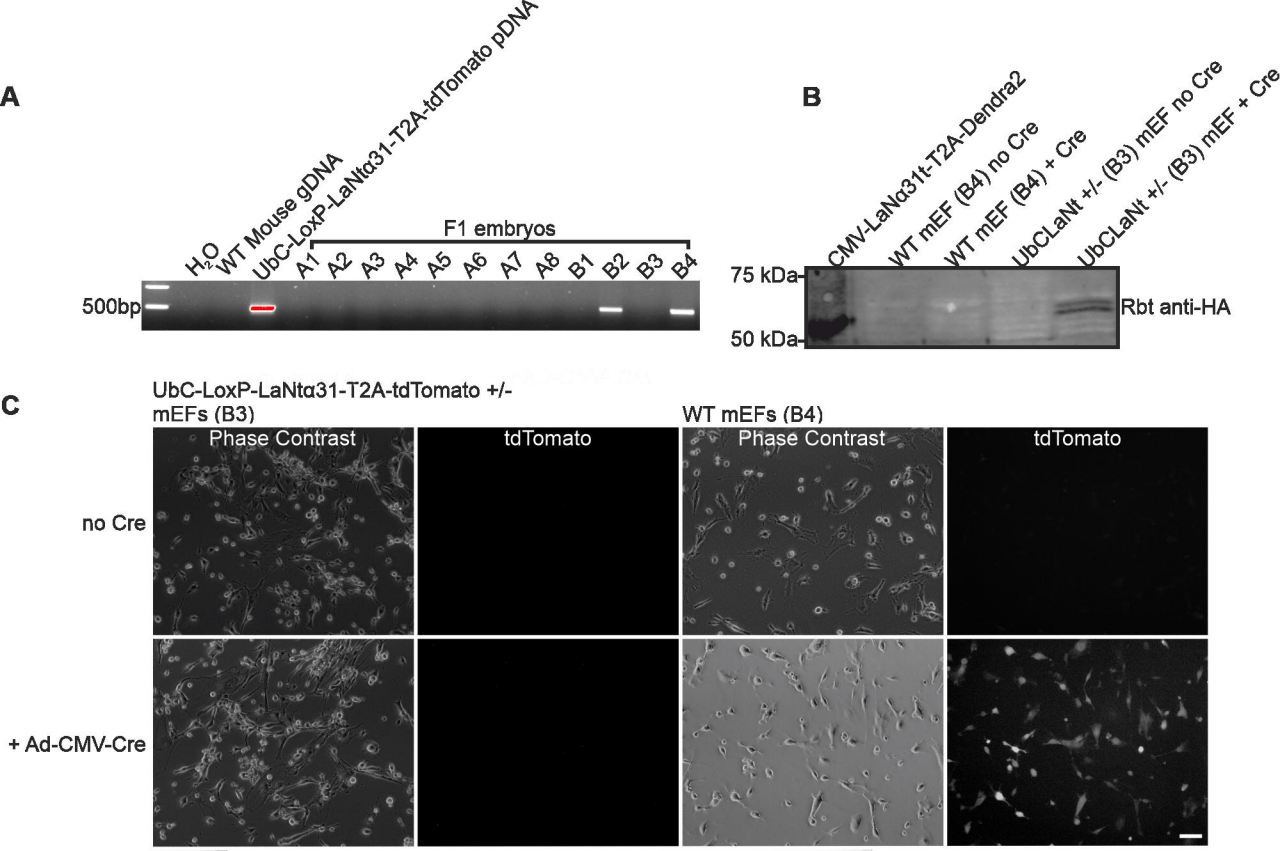
A
H2O
WT Mouse gDNA
UbC-LoxP-LaNtα31-T2A-tdTomato pDNA
F1 embryos
A1
A2
A3
A4
A5
A6
A7
A8
B1
B2
B3
B4
500bp
B
CMV-LaNα31t-T2A-Dendra2
WT mEF (B4) no Cre
WT mEF (B4) + Cre
UbCLaNt +/- (B3) mEF no Cre
UbCLaNt +/- (B3) mEF + Cre
75 kDa
50 kDa
Rbt anti-HA
C
UbC-LoxP-LaNtα31-T2A-tdTomato +/- mEFs (B3)
WT mEFs (B4)
Phase Contrast
tdTomato
Phase Contrast
tdTomato
no Cre
+ Ad-CMV-Cre

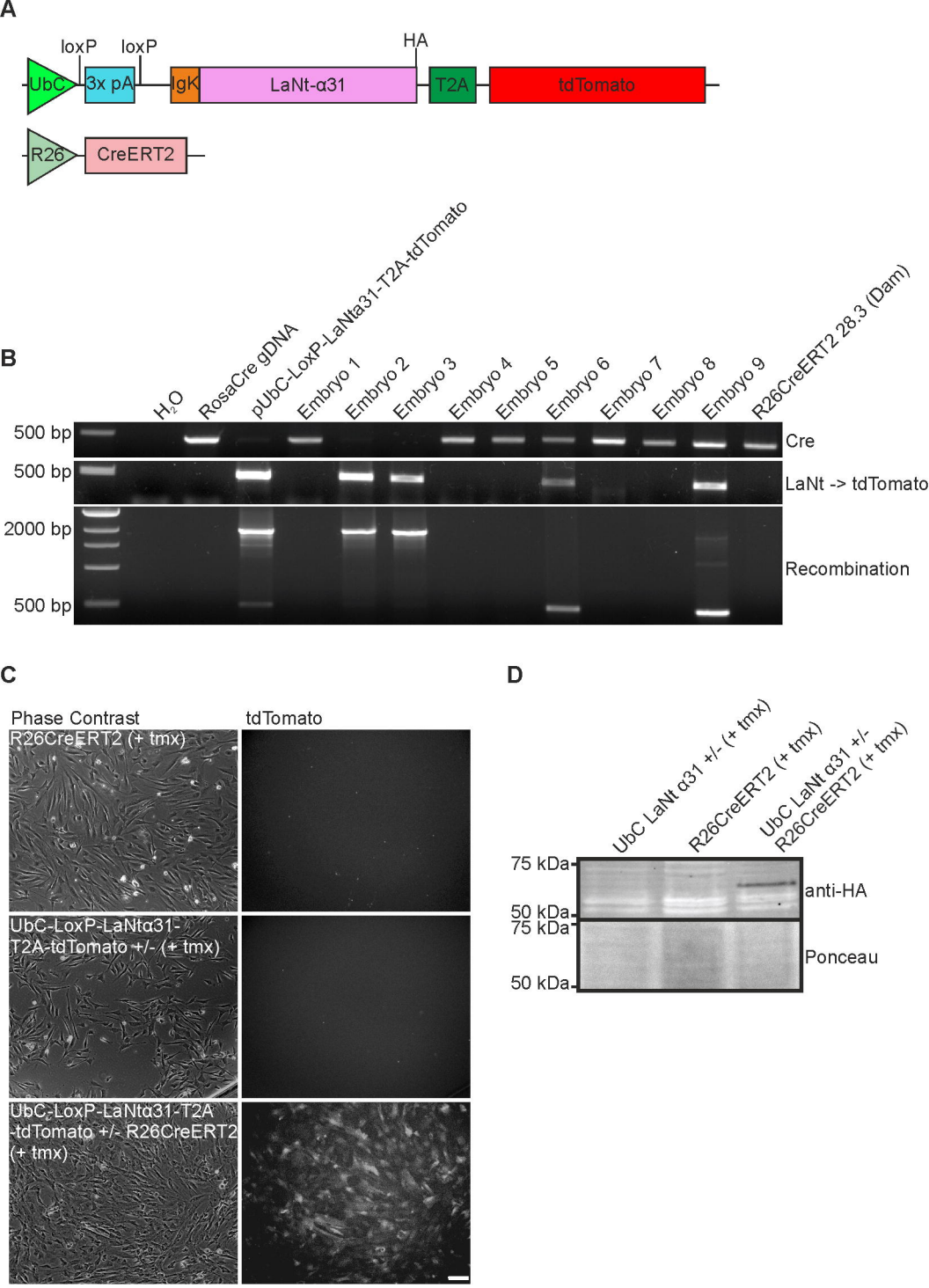
A
loxP
loxP
HA
UbC
3x pA
IgK
LaNt-α31
T2A
tdTomato
R26
CreERT2
B
H2O
RosaCre gDNA
pUbC-LoxP-LaNta31-T2A-tdTomato
Embryo 1
Embryo 2
Embryo 3
Embryo 4
Embryo 5
Embryo 6
Embryo 7
Embryo 8
Embryo 9
R26CreERT2 28.3 (Dam)
500 bp
Cre
500 bp
LaNt -> tdTomato
2000 bp
Recombination
500 bp
C
Phase Contrast
tdTomato
R26CreERT2 (+ tmx)
UbC-LoxP-LaNtα31-T2A-tdTomato +/- (+ tmx)
UbC-LoxP-LaNtα31-T2A-tdTomato +/- R26CreERT2 (+ tmx)
D
UbC LaNt α31 +/- (+ tmx)
R26CreERT2 (+ tmx)
UbC LaNt α31 +/- R26CreERT2 (+ tmx)
75 kDa
anti-HA
50 kDa
75 kDa
Ponceau
50 kDa

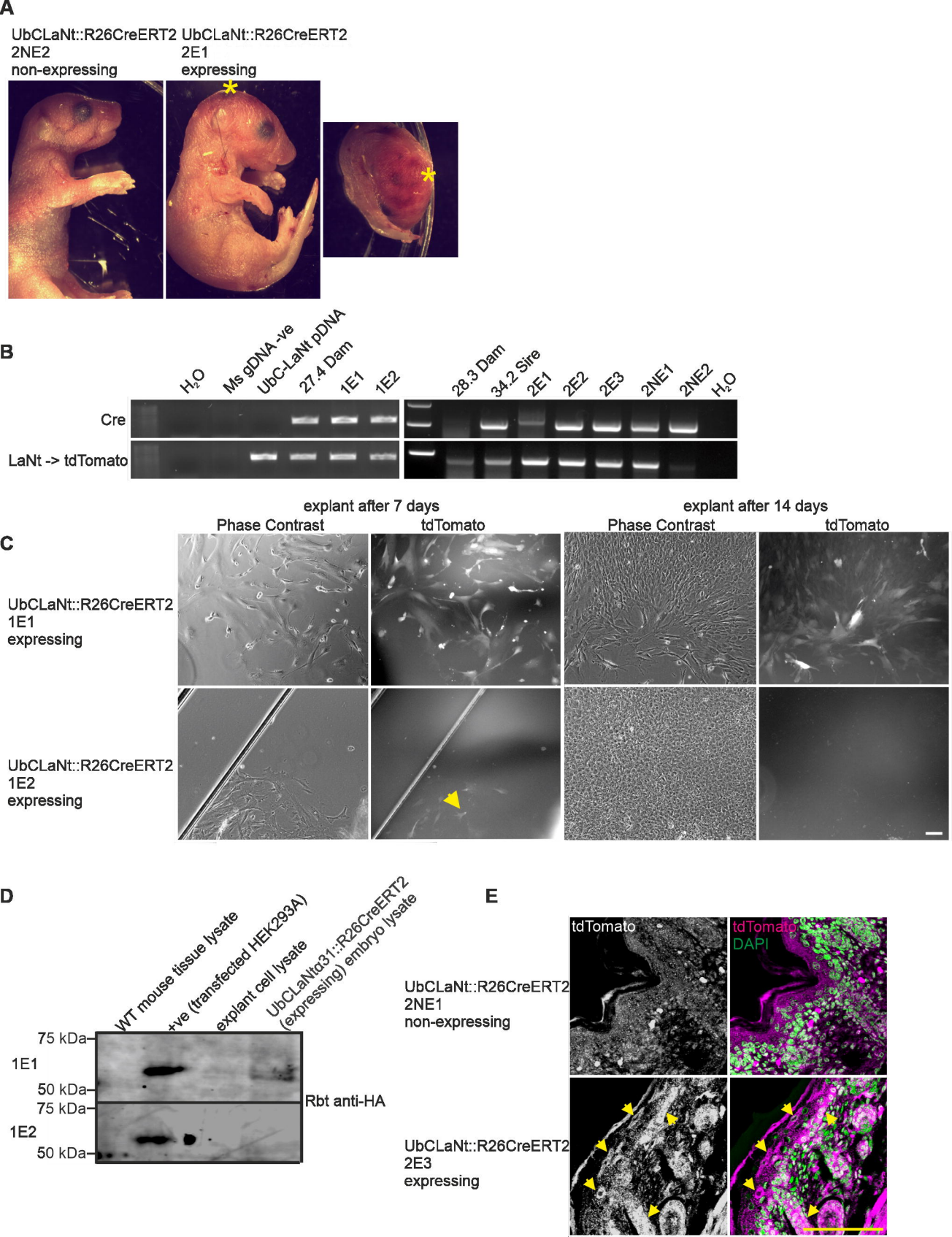
A
UbCLaNt::R26CreERT2
2NE2
non-expressing
UbCLaNt::R26CreERT2
2E1
expressing
B
H2O
Ms gDNA -ve
UbC-LaNt pDNA
27.4 Dam
1E1
1E2
28.3 Dam
34.2 Sire
2E1
2E2
2E3
2NE1
2NE2
H2O
Cre
LaNt -> tdTomato
C
explant after 7 days
Phase Contrast
tdTomato
explant after 14 days
Phase Contrast
tdTomato
UbCLaNt::R26CreERT2
1E1
expressing
UbCLaNt::R26CreERT2
1E2
expressing
D
WT mouse tissue lysate
+ve (transfected HEK293A)
explant cell lysate
UbCLaNtα31::R26CreERT2
(expressing) embryo lysate
75 kDa
1E1
50 kDa
75 kDa
1E2
50 kDa
Rbt anti-HA
E
tdTomato
tdTomato
DAPI
UbCLaNt::R26CreERT2
2NE1
non-expressing
UbCLaNt::R26CreERT2
2E3
expressing

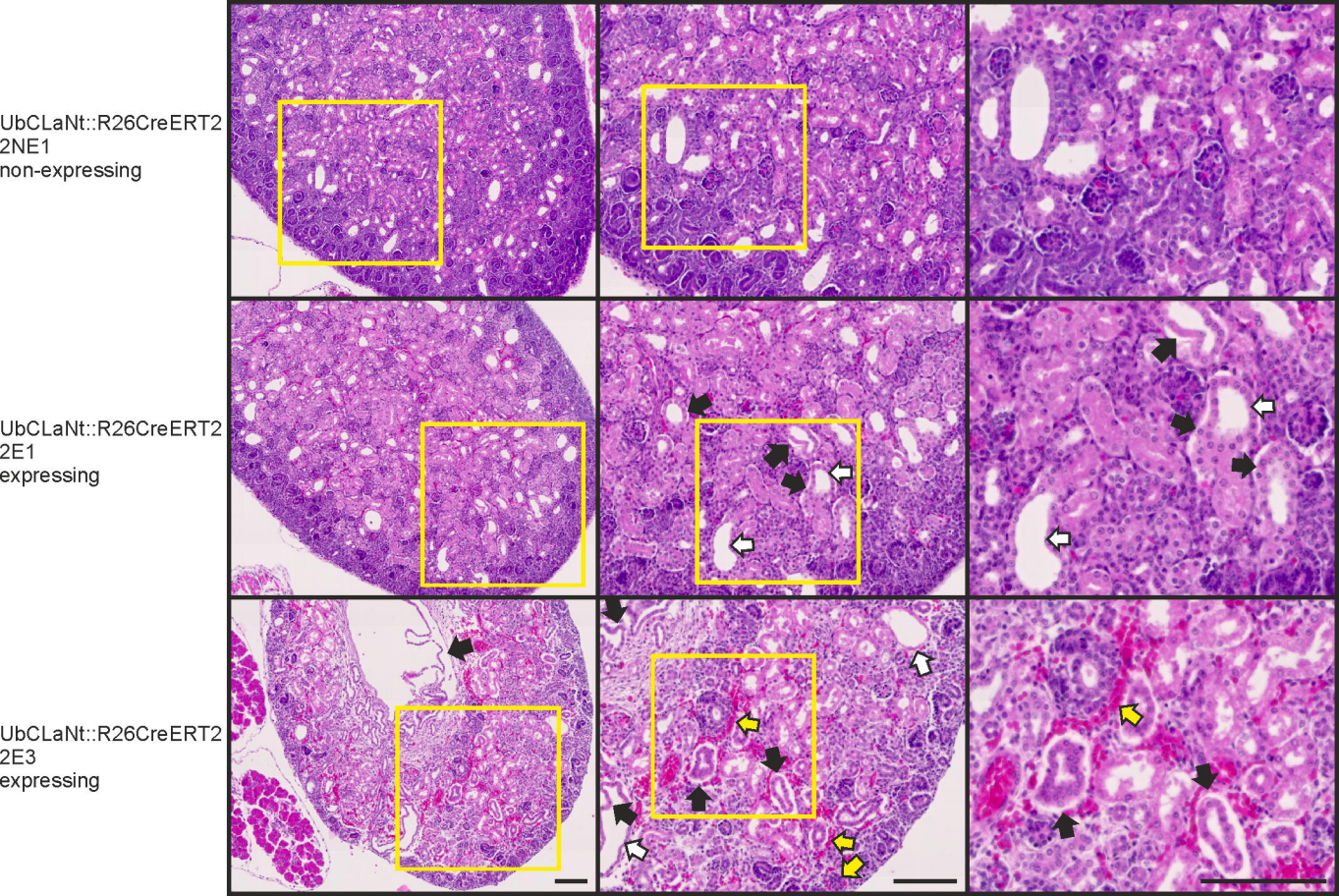
UbCLaNt::R26CreERT2
2NE1
non-expressing
UbCLaNt::R26CreERT2
2E1
expressing
UbCLaNt::R26CreERT2
2E3
expressing

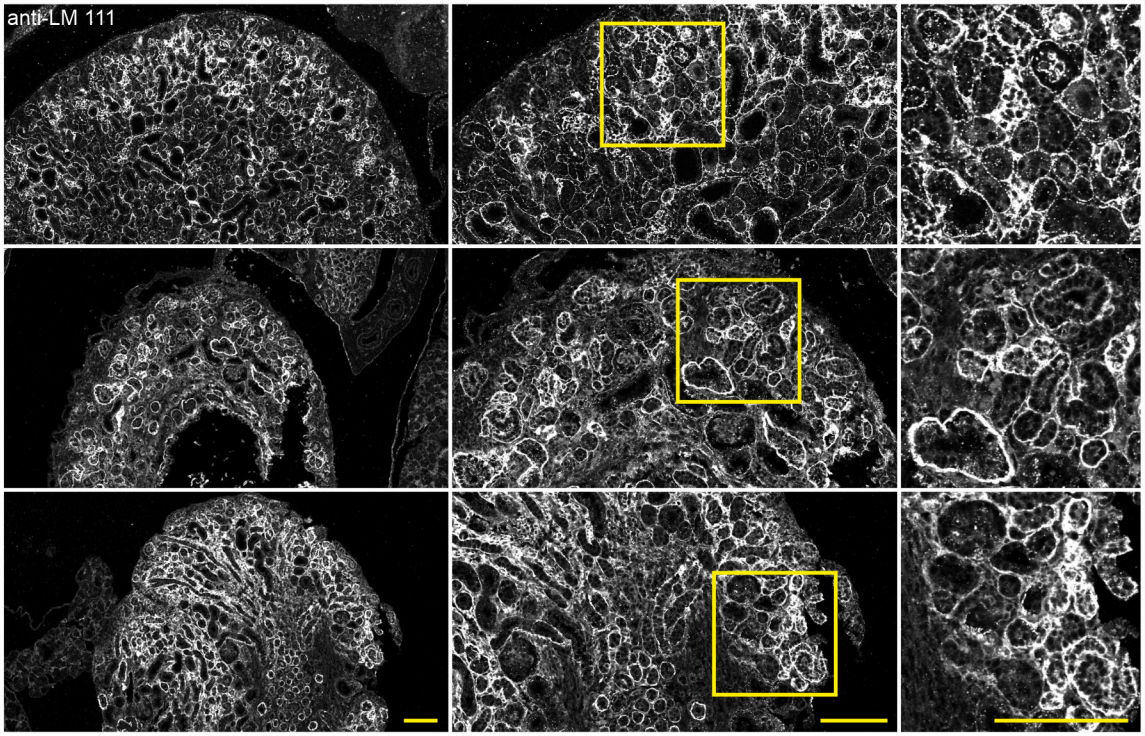
anti-LM 111
UbCLaNt::R26CreERT2
2NE1
non-expressing
UbCLaNt::R26CreERT2
2E1
expressing
UbCLaNt::R26CreERT2
2E3
expressing

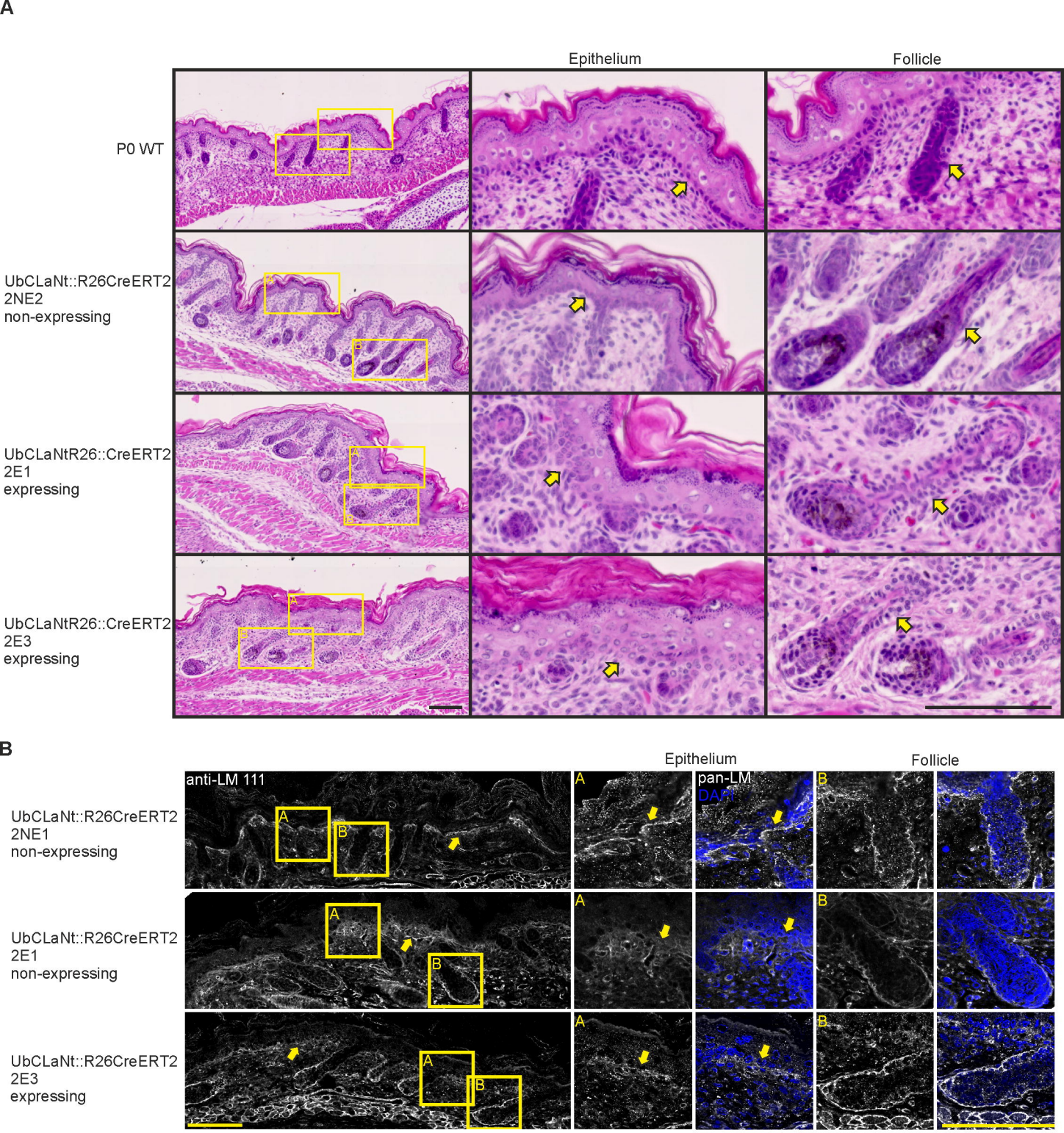
A
Epithelium
Follicle
P0 WT
UbCLaNt::R26CreERT2
2NE2
non-expressing
UbCLaNtR26::CreERT2
2E1
expressing
UbCLaNtR26::CreERT2
2E3
expressing
B
Epithelium
Follicle
anti-LM 111
pan-LM
DAPI
UbCLaNt::R26CreERT2
2NE1
non-expressing
UbCLaNt::R26CreERT2
2E1
non-expressing
UbCLaNt::R26CreERT2
2E3
expressing

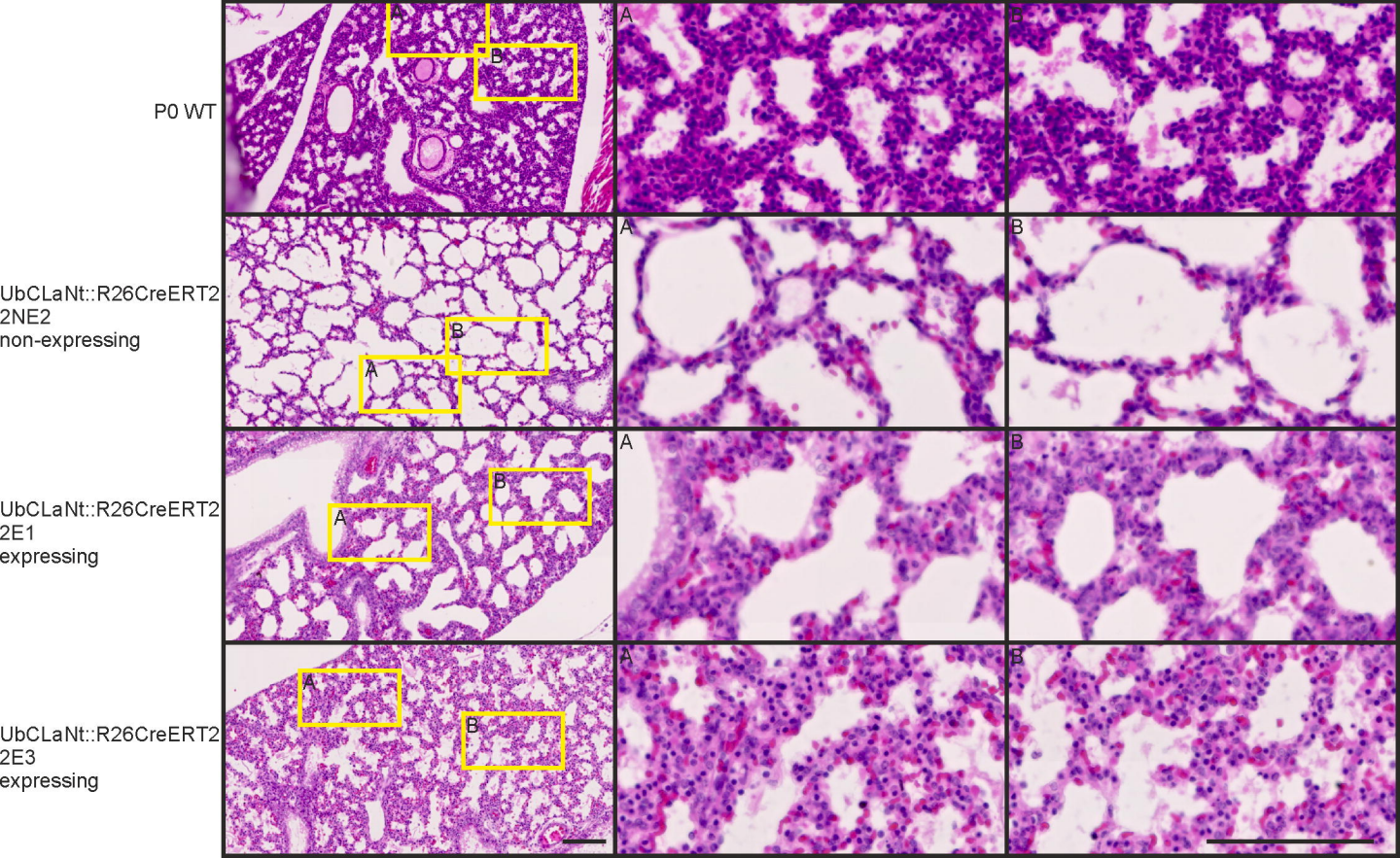
P0 WT
UbCLaNt::R26CreERT2
2NE2
non-expressing
UbCLaNt::R26CreERT2
2E1
expressing
UbCLaNt::R26CreERT2
2E3
expressing
A
B

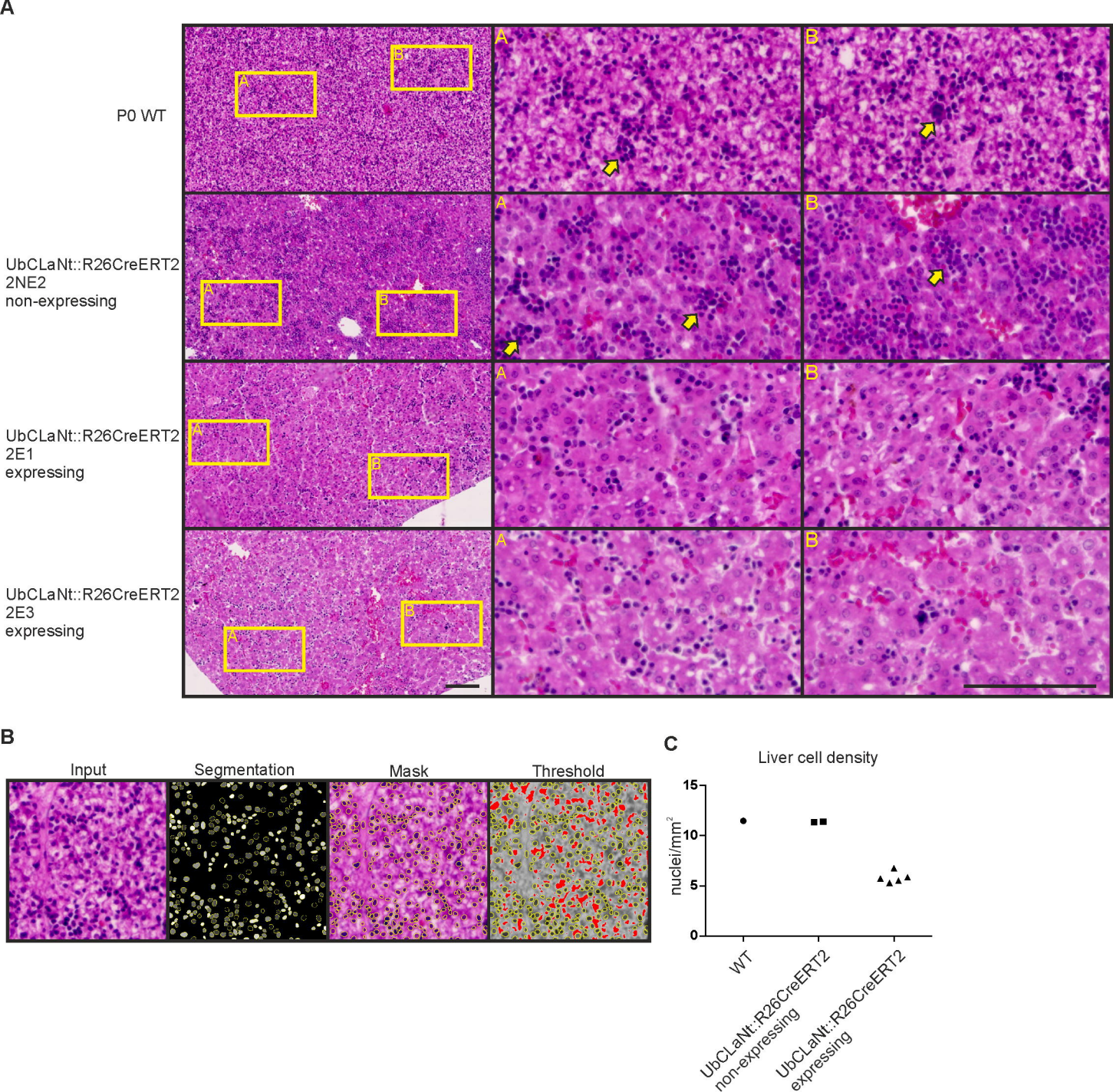
A
P0 WT
UbCLaNt::R26CreERT2
2NE2
non-expressing
UbCLaNt::R26CreERT2
2E1
expressing
UbCLaNt::R26CreERT2
2E3
expressing
A
B
B
Input
Segmentation
Mask
Threshold
C
Liver cell density
nuclei/mm2
15
10
5
0
WT
UbCLaNt::R26CreERT2
non-expressing
UbCLaNt::R26CreERT2
expressing